

CrossMark  
click for updates

Cite this: DOI: 10.1039/c6ta02593e

# Excellent low temperature performance for total benzene oxidation over mesoporous CoMnAl composited oxides from hydrotalcites†

Shengpeng Mo,<sup>ab</sup> Shuangde Li,<sup>a</sup> Wenhui Li,<sup>ab</sup> Jiaqi Li,<sup>ab</sup> Jiayuan Chen<sup>ab</sup>  
and Yunfa Chen<sup>\*a</sup>

Mesoporous CoMnAl mixed metal oxide catalysts with various Co/Mn atomic ratios have been obtained by calcination at 450 °C of layered double hydroxide (LDH) precursors prepared by the NH<sub>4</sub>OH co-precipitation–hydrothermal method without distinct MnCO<sub>3</sub> peaks. The catalysts exhibited high efficiency for total oxidation of volatile organic compounds (VOCs). The physicochemical properties of the catalysts were characterized using several analytical techniques. Among them, CoMn<sub>2</sub>AlO shows the optimal activity and the temperature required to achieve a benzene conversion of 90% ( $T_{90}$ ) was about 238 °C, with a reaction rate and activity energy ( $E_a$ ) of 0.24 mmol g<sub>cat</sub><sup>-1</sup> h<sup>-1</sup> and 65.77 kJ mol<sup>-1</sup> respectively. This temperature was 47 °C lower than that on the Co<sub>3</sub>AlO sample with a lower reaction rate of 0.19 mmol g<sub>cat</sub><sup>-1</sup> h<sup>-1</sup> and a higher  $E_a$  130.31 kJ mol<sup>-1</sup> at a high space velocity (SV = 60 000 mL g<sup>-1</sup> h<sup>-1</sup>). The effects of calcination temperature on the textural properties and catalytic activity of the CoMn<sub>2</sub>AlO catalyst were further investigated. The as-prepared CoMn<sub>2</sub>AlO-550 sample displayed superior catalytic activity, with  $T_{90}$  at 208 °C, compared CoMn<sub>2</sub>AlO-450. The formation of a solid solution with high surface area, rich oxygen vacancies, high Mn<sup>4+</sup>/Mn<sup>3+</sup> and Co<sup>3+</sup>/Co<sup>2+</sup> ratios and low-temperature reducibility made a great contribution to the significant improvement of the catalytic activity.

Received 29th March 2016  
Accepted 9th May 2016

DOI: 10.1039/c6ta02593e

www.rsc.org/MaterialsA

## 1. Introduction

Volatile organic compounds (VOCs) are one of the main air pollutants emitted from industrial processes and the combustion of fossil fuels; they may pollute the atmosphere directly or indirectly as secondary pollutants, such as ozone formation and photochemical smog.<sup>1</sup> Indoor VOCs emitted from cement concrete, furniture and paint also have become an increasingly common concern over the past several years, as they cause bad indoor air quality (IAQ) together with indoor microbes and particulates which can be found at higher concentrations indoors than outdoors.<sup>2,3</sup> Lowering the concentration of VOCs and their associated photochemical impacts on human health has become a major issue.<sup>4</sup> Therefore, it is highly desirable to efficiently and cost-effectively remove hazardous VOCs. Many technologies for VOC abatement (*e.g.* adsorption, thermal oxidation and catalytic oxidation) have been developed in the last few decades: catalytic oxidation is regarded as an effective

method for VOC abatement, due to its lower operating temperature and less harmful reaction by-products than thermal oxidation.<sup>5</sup> Noble metals and transition metal oxides are commonly used for the catalytic oxidation of VOCs. Though supported noble metal catalysts (Pt, Pd, Au and Ag) exhibit higher activity for deep oxidation of VOCs at very low temperatures, their high cost, easy sintering and coking, and susceptibility to poisoning have limited their wide and abundant usage. The key issue is the availability of a low-cost catalyst with high activity in catalytic oxidation technology. Thus, substantial efforts are currently being made to develop transition metal oxide catalysts (Co<sub>3</sub>O<sub>4</sub>, NiO, Cr<sub>2</sub>O<sub>3</sub>, CuO and MnO<sub>2</sub>) which may be expected to be better alternatives to the precious metal catalysts.

Previous studies revealed that mixed metal oxides (*e.g.* Mn–Co–O,<sup>6,7</sup> Mn–Ce–O,<sup>8,9</sup> Mn–Ni–O,<sup>10</sup> Co–Ce–O,<sup>11,12</sup>) possess improved catalytic activities compared to single-component materials due to synergistic effects. There are frequently weaker interactions between mixed metal oxides, which decrease their catalytic activity and stability, and their resistance to water vapor. Thus, there are still challenges and opportunities in developing synergistic effects for mixed metal oxide catalysts with high catalytic activity. Recently, many reports have contributed to the synthesis, characterization, and catalytic applications of mixed oxides produced by thermal decomposition of layered double hydroxides (LDHs), such as Mn–Al,<sup>13</sup> Cu–Co–Al,<sup>14</sup> and Co–Mg–Al.<sup>15</sup>

<sup>a</sup>State Key Laboratory of Multi-phase Complex Systems, Institute of Process Engineering, Chinese Academy of Sciences, Beijing, 100190, China. E-mail: yfchen@mail.ipe.ac.cn; chemyf@ipe.ac.cn; Fax: +86 10 8254 4896; Tel: +86 10 8254 4896

<sup>b</sup>University of Chinese Academy of Sciences, Beijing 100049, PR China

† Electronic supplementary information (ESI) available: SEM image, element distribution and EDX data of the Co<sub>3</sub>AlO, Co<sub>2</sub>MnAlO and Mn<sub>3</sub>AlO sample, CO<sub>2</sub> conversion and analysis of exhausted gas. See DOI: 10.1039/c6ta02593e

Layered double hydroxides, known as hydroxide-like compounds or anionic clays, are a class of two-dimensional (2D) layered inorganic materials, which can be represented by the general chemical formula  $[M_{1-x}^{2+}M_x^{3+}(\text{OH})_2](A^{n-})_{x/n} \cdot m\text{H}_2\text{O}$ , where  $M^{2+}$  and  $M^{3+}$  represent metallic cations,  $A^{n-}$  indicates interlayer anions such as  $\text{NO}_3^-$  or  $\text{CO}_3^{2-}$ ,  $x$  is the molar ratio of  $M^{3+}/(M^{2+} + M^{3+})$  and  $m$  represents the amount of water.<sup>16,17</sup> A unique structural characteristic of LDH materials is that the  $M^{2+}$  and  $M^{3+}$  are distributed in an ordered and uniform manner in brucite-like layers. Mixed oxide catalysts obtained by controlled thermal decomposition of LDHs have two advantages: (1) they are effective supports for the immobilization of catalytically active species on the surface and (2) the uniform dispersion of  $M^{2+}$  and  $M^{3+}$  cations in the layers can act as excellent solid base catalysts. Co–Mn–Al mixed oxides with high specific surface areas synthesized using co-precipitation techniques improved the catalytic activity towards toluene oxidation, and can be an excellent alternative to noble metal catalysts.<sup>18</sup> Forming hybrid oxide catalysts with hierarchical structure from the calcination of their LDH precursors offers the benefits of synergistic effects between the metal oxide materials and further enhances the catalytic activity and stability. Consequently, the rational design and controllable preparation of mixed metal oxide catalysts based on LDH materials with simultaneously enhanced activity and stability is of great interest.<sup>17</sup>

The use of LDH powdered catalysts presents problems because of mass/heat transfer resistance, as well as the difficulty in recycling. An approach of growing an LDH support on aluminum foil<sup>19</sup> has been attracting considerable attention: it affords a structured catalyst with excellent mass flow properties and recyclability, as well as high thermal conductivity. Kovanda<sup>20</sup> synthesized layers of Co–Mn–Al mixed oxides supported on anodized aluminum foil which showed slightly higher specific activity in the total oxidation of ethanol. We previously fabricated a monolithic CuCoAl MMO film catalyst by an *in situ* growth–calcination method, which displayed comparable catalytic activity to  $\text{Cu}_x\text{Co}_{3-x}\text{Al}$  MMO powder for the catalytic oxidation of benzene.<sup>14</sup> In the present work, we consider that Mn and Co mixed oxides are valuable materials in oxidation reactions due to their ability to exist in multiple oxidation states and optimum oxygen storage capacity. To investigate systematically the effect of Co (or Mn) substitution, we have prepared CoMnAlO powdered mixed metal oxide catalysts derived from LDHs with high synergistic effect, which significantly promoted the activity towards benzene combustion, and are resistant to large amounts of water vapor. Moreover, we have successfully fabricated a monolithic highly dispersed CoMnAlO film catalyst by an *in situ* growth–calcination method with outstanding performance to replace powder samples.

## 2. Experimental

### 2.1 Synthesis of $\text{Co}_{3-x}\text{Mn}_x\text{Al}$ LDHs

The synthesis of LDH precursor samples (with Co/Mn molar ratios of 3/0, 2/1, 1.5/1.5, 1/2, 0/3 and  $M^{2+}/M^{3+}$  molar ratio of 3/1) was based on the co-precipitation–hydrothermal method.

Firstly, a solution of  $\text{Co}(\text{NO}_3)_2 \cdot 6\text{H}_2\text{O}$ ,  $\text{Mn}(\text{NO}_3)_2$  ( $\text{Co}^{2+} + \text{Mn}^{2+} = 15$  mmol) and  $\text{Al}(\text{NO}_3)_3 \cdot 9\text{H}_2\text{O}$  (5 mmol) dissolved in 70 mL of deionized water was produced. Secondly,  $\text{NH}_4\text{OH}$  (water solution 25%) was added dropwise to the mixed nitrate salt solution with constant agitation, keeping at a constant pH value of 9.0. Thirdly, the obtained precipitate was transferred to a Teflon autoclave at 120 °C for 6 h. Subsequently, the obtained precipitate was centrifuged, washed with deionized water and ethanol, and then dried at 80 °C overnight.

### 2.2 Preparation of $\text{Co}_{3-x}\text{Mn}_x\text{AlO}$ samples

The  $\text{Co}_{3-x}\text{Mn}_x\text{Al}$  LDHs samples were calcined in air at 450 °C for 4 h at a heating rate of 2 °C  $\text{min}^{-1}$  (denoted as  $\text{Co}_{3-x}\text{Mn}_x\text{AlO}$ ). The effect of calcination in air at different temperatures (350 or 550 °C) on the catalyst performance was then investigated (resulting samples denoted as  $\text{Co}_{3-x}\text{Mn}_x\text{AlO-350}$ ,  $\text{Co}_{3-x}\text{Mn}_x\text{AlO-550}$ , respectively).

### 2.3 Preparation of monolithic CoMnAlO film catalyst

CoMnAl LDH film was prepared by *in situ* crystallization on a pure aluminum substrate. In a typical procedure, 10 mmol of  $\text{Mn}(\text{NO}_3)_2$  and 5 mmol of  $\text{Co}(\text{NO}_3)_2 \cdot 6\text{H}_2\text{O}$  were dissolved in deionized water to form a clear solution with a total volume of 70 mL, the pH value was adjusted to 9.0 by adding diluted ammonia (25 wt%  $\text{NH}_4\text{OH}$ ). Three pieces of Al substrate ( $4 \times 15$  cm) were rolled into a tubular shape and immersed vertically in the solution, and were then cleaned with acetone, ethanol and deionized water in sequence before use. They were transferred to a Teflon autoclave placed in an oven at 120 °C for 12 h. The substrates were taken out of the autoclave, rinsed with deionized water and dried at room temperature. Then the as-prepared CoMnAl LDH film was heated at 550 °C for 4 h at 2 °C  $\text{min}^{-1}$  (denoted as CoMnAlO film).

### 2.4 Characterization of the catalysts

The powder X-ray diffraction (XRD) patterns were measured on a Panalytical X'Pert PRO system within the range of scattering angle  $2\theta$  of 5–90°.  $\text{N}_2$  adsorption/desorption isotherms were measured *via*  $\text{N}_2$  adsorption at 77 K on an automatic surface analyzer (SSA-7300, China), and the BET specific surface areas and pore size distributions were obtained according to the Brunauer–Emmett–Teller (BET) and Barrett–Joyner–Halenda (BJH) methods, respectively. The morphology and microstructures were recorded on a scanning electron microscope (SEM, JEOL JSM-6700F, Japan, 15 kV, 10 mM) and transmission electron microscope (TEM, JEOL JEM-2010F, 200 kV). Hydrogen temperature programmed reduction ( $\text{H}_2$ -TPR) with 20 mg catalyst (40–60 mesh) was carried out in a U-shaped quartz reactor under a gas flow (10%  $\text{H}_2$  balanced with Ar, 25 mL  $\text{min}^{-1}$ ) at a constant rate of 10 °C  $\text{min}^{-1}$ . Surface species of the as-prepared catalysts were determined by X-ray photoelectron spectroscopy (XPS) using an XLESCALAB 250Xi electron spectrometer from VG Scientific with monochromatic Al K $\alpha$  radiation.

## 2.5 Catalytic activity measurement

The catalytic activity was evaluated in a continuous-fixed-bed quartz microreactor ( $\varphi = 6$  mm) at a space velocity (SV) of 60 000 mL g<sup>-1</sup> h<sup>-1</sup>. The catalysts (100 mg, 40–60 mesh) mixed with 200 mg of quartz sand (40–60 mesh) were loaded in the quartz reactor with quartz wool packed at both ends of the catalyst bed. The reactant gas was composed of 100 ppm gaseous benzene balanced with air (20% O<sub>2</sub> + balance N<sub>2</sub>), which was purged into the reactor at a continuous flow of 100 mL min<sup>-1</sup>. The concentration of benzene was analyzed using a gas chromatograph (Shimadzu GC-2014) equipped with a flame ionization detector (FID) and the concentration of CO<sub>2</sub> in the outlet gas was detected by another FID with a conversion furnace for converting CO<sub>2</sub> to CH<sub>4</sub>. The catalytic evaluation of the CoMnAlO film catalyst on the Al substrate was performed on pre-tailored fragments (1 × 5 cm) which were rolled into a tubular shape. The complete conversion value of benzene ( $\eta_{\text{benzene}}$ ) was calculated according to the following equations:

$$\eta_{\text{benzene}} = \frac{C_{\text{benzene,in}} - C_{\text{benzene,out}}}{C_{\text{benzene,in}}} \times 100$$

$$\eta_{\text{CO}_2} = \frac{C_{\text{CO}_2,\text{out}}}{6 \times C_{\text{benzene,in}}} \times 100$$

where  $C_{\text{benzene,in}}$  (ppm),  $C_{\text{benzene,out}}$  (ppm) and  $C_{\text{CO}_2,\text{out}}$  (ppm) are the concentrations of benzene in the inlet and outlet gases, and CO<sub>2</sub> in the outlet gas, respectively.

To investigate the effect of water vapor on the catalytic activity, the on-stream benzene oxidation experiment was carried out in the presence and absence of 7.2 vol% water vapor. Typically, an air flow containing gaseous benzene (100 mL min<sup>-1</sup>) was used for bubbling through water in a 500 mL conical flask at 40 °C to give a water vapor amount of 7.2 vol%, and benzene (100 ppm) was used for catalytic testing.

## 3. Results and discussion

### 3.1 Textural study of the precursors and catalysts

The XRD patterns of Co<sub>3-x</sub>Mn<sub>x</sub>Al LDHs precursors are shown in Fig. 1(A and B). In the material prepared by co-precipitation, the XRD patterns clearly exhibit the characteristic reflections of LDH materials with a series of (00*l*) peaks, indicating the generation of a layered structure with 3*R* symmetry. In the case of using NO<sub>3</sub><sup>-</sup> as a guest anion, the lattice parameter  $a = 2 \times d(110)$  around  $2\theta = 58.5^\circ$ , intense diffraction peaks ( $d(003) = 0.86$  nm and  $d(006) = 0.44$  nm) were observed with Mn<sub>3</sub>Al LDH structure, while  $c = 3 \times d(003)$  around  $2\theta = 10.3^\circ$ , which is a function of the interlayer distance.<sup>21</sup> For Co<sub>3</sub>Al LDH, diffraction peaks located at 10.8° and 21.6° are observed, corresponding to the (003) and (006) planes, respectively.<sup>22</sup> In addition, cobalt ammine azide formation is possible even if NH<sub>4</sub>OH solution was employed during the preparation. As shown in Fig. 1(B), the low angle shift of the peaks indicates that the increase in the lattice distance results from doping with Mn<sup>2+</sup> which possesses a large radius (0.74 Å for Co<sup>2+</sup> vs. 0.83 Å

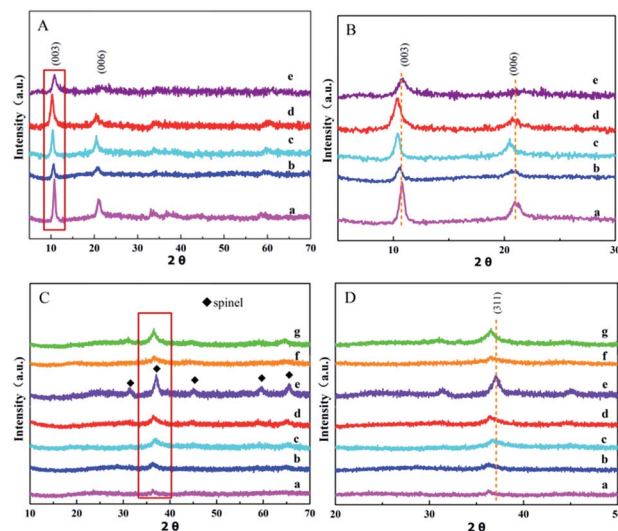


Fig. 1 (A and B) (a–e) XRD patterns of Mn<sub>3</sub>Al, CoMn<sub>2</sub>Al, Co<sub>1.5</sub>Mn<sub>1.5</sub>Al, Co<sub>2</sub>MnAl, Co<sub>3</sub>Al LDH precursors; (C and D) (a–g) XRD patterns of Mn<sub>3</sub>AlO, CoMn<sub>2</sub>AlO, Co<sub>1.5</sub>Mn<sub>1.5</sub>AlO, Co<sub>2</sub>MnAlO, Co<sub>3</sub>AlO, CoMn<sub>2</sub>AlO-350 and CoMn<sub>2</sub>AlO-550 catalysts.

for Mn<sup>2+</sup>, respectively) in an octahedral environment.<sup>23</sup> The XRD results also indicate that the single phase of the NO<sub>3</sub><sup>-</sup>/Co<sub>3-x</sub>Mn<sub>x</sub>Al LDHs can be synthesized by the NH<sub>4</sub>OH co-precipitation method without any distinct peaks corresponding to the MnCO<sub>3</sub> (rhodochrosite) admixture commonly produced with the NaOH and Na<sub>2</sub>CO<sub>3</sub>/K<sub>2</sub>CO<sub>3</sub> co-precipitation method.<sup>15</sup>

After calcination in air at 450 °C, the LDH precursors were completely transformed to a mixture of oxide and spinel oxide phases. The XRD patterns of Co<sub>3-x</sub>Mn<sub>x</sub>AlO are shown in Fig. 1(C and D). It can be clearly seen that the positions and relative intensities of the main diffraction peaks of the samples are rather similar. The strongest reflection at  $2\theta = 36.8^\circ$  corresponds to a Co<sub>3</sub>O<sub>4</sub> spinel phase (PDF card no. 42-1467) in Fig. 1(B)(e), and the Co<sub>3</sub>AlO sample is observed with other weak diffraction peaks located at 31.3°, 44.9°, 59.4° and 65.4°, corresponding to the (220), (400), (511) and (440) planes, respectively. Furthermore, the main diffraction peaks of the Co<sub>3</sub>AlO sample are rather similar to those of other spinel oxide phases (Co<sub>2</sub>AlO<sub>4</sub>, PDF card no. 38-0814; CoAl<sub>2</sub>O<sub>4</sub>, PDF card no. 44-0160), which are hard to distinguish by X-ray diffraction.<sup>24,25</sup> The formation of Co<sub>3</sub>O<sub>4</sub> is due to the easy oxidation potential of Co<sup>2+</sup> ions and the thermodynamic stability of Co<sub>3</sub>O<sub>4</sub>, higher than that of CoO in air.<sup>18</sup> As the cobalt content is decreased, the intensities of the Co<sub>3</sub>O<sub>4</sub> peaks decrease and the peaks become weak. The XRD pattern of Mn<sub>3</sub>AlO (Fig. 1(C)(b)) shows complex diffraction peaks, which are ascribed to a mixture of lower-crystalline Mn<sub>5</sub>O<sub>8</sub> (JCPDS 18-0801) and Mn<sub>3</sub>O<sub>4</sub> (JCPDS 02-1062). After addition of cobalt species into MnAl precursors, a typical diffraction peak of their mixed oxides around 36.5° appears which may be ascribed to the formation of cobalt manganese oxide (JCPDS 018-0410) with spinel structure or a new cobalt aluminum manganese oxide (CoMnAlO<sub>4</sub>, JCPDS 036-0269) homogeneous crystal phase. The XRD patterns of CoMn<sub>2</sub>AlO samples at different calcination temperatures are shown in

Fig. 1(D)(b, f and g), the intensities of the peaks increase with increasing calcination temperature. When the calcination temperature is increased to 550 °C, the formation of a solid solution can obviously improve the catalytic activities due to the synergistic effect of the components.<sup>26</sup> The average crystalline sizes calculated by using the Scherrer equation are listed in Table 1. With increasing the Co species into the MnAl lamellar structure, the grain size of crystallites is significantly increased. The size of CoMn<sub>2</sub>Al is 14.6 nm which is smallest among other samples prepared by calcination at 450 °C. This result further indicates that the formation of a solid solution between Co and Mn oxides indeed can decrease the size of crystallites compared to the single Co<sub>3</sub>AlO (24.9 nm). Small-sized particles will produce more crystal defects which are beneficial to catalytic activity.

Fig. 2(A) displays the N<sub>2</sub> adsorption/desorption isotherms and the pore size distribution patterns for the Co<sub>3-x</sub>Mn<sub>x</sub>AlO catalysts. The isotherms are consistent with type IV isotherms with a H2-type hysteresis loop in the relative pressure range of 0.4–1.0, which are associated with capillary condensation taking place in mesopores and confirmed by the distribution of pore size in Fig. 2(B). The surface area, pore volume and pore diameter of all the samples are shown in Table 1. When Co<sup>2+</sup> is incorporated more efficiently into the layered structure, they have larger surface areas around 120–130 m<sup>2</sup> g<sup>-1</sup> for Co<sub>3-x</sub>Mn<sub>x</sub>AlO catalysts compared with those of Co<sub>3</sub>AlO and Mn<sub>3</sub>AlO catalysts (about 84.63 and 36.77 m<sup>2</sup> g<sup>-1</sup>). It is noticeable that the average pore size distributions become narrower for CoMn<sub>2</sub>AlO with 7.1 nm than other samples with 8–24 nm. The accessibility of nitrogen gas to the particle interior varied depending upon the particle size. For large-sized particles, nitrogen gas cannot easily access the active sites of the particles with a low surface area.<sup>27,28</sup> These results indicate that Co<sup>2+</sup> substitution in the brucite layer leads to changes in the surface properties of Mn<sub>3</sub>AlO and can lead to improvements in the catalytic activity for benzene oxidation. The effect of calcination temperature on CoMn<sub>2</sub>AlO samples was also examined. The surface area gradually decreased from 143.8, 128.0 to 102.4 m<sup>2</sup> g<sup>-1</sup>, together with increased pore size distribution, with enhanced calcination temperature from 350, 450 to 550 °C.

### 3.2 Morphology, microstructure and element distribution

The SEM pictures of the Co<sub>3-x</sub>Mn<sub>x</sub>Al LDHs particles are shown in Fig. 3. These shapes approximate to thin hexagonal platelets

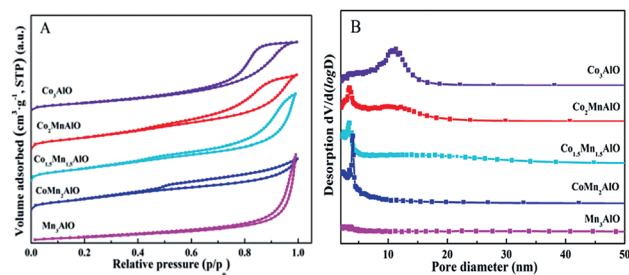


Fig. 2 (A) N<sub>2</sub> adsorption/desorption isotherms and (B) pore-size distributions for the Co<sub>3-x</sub>Mn<sub>x</sub>AlO catalysts.

with high aspect ratio flakes. The as-prepared Mn<sub>3</sub>Al LDH product is of higher quality in terms of morphology, size, uniformity, and crystallinity, which is much superior to those of Co<sub>3</sub>Al LDH. These results are consistent with the X-ray diffraction peak intensity between Co<sub>3</sub>Al LDH and Mn<sub>3</sub>Al LDH samples. As shown in Fig. 3(B), the particle size of CoMn<sub>2</sub>Al LDH is slightly different from the samples including alternating Co and Mn metal ions, indicating that when Co<sup>2+</sup> is incorporated efficiently into the layered structure, the morphology and size of particles are changed. The SEM images of CoMn<sub>2</sub>AlO after calcination in air at different temperatures are shown in Fig. 3(D–F). The morphology of CoMn<sub>2</sub>Al LDH can maintain a relatively complete shape after calcination in air at 350 °C,

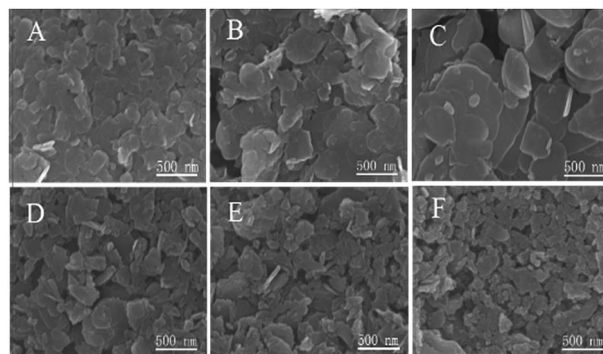


Fig. 3 (A–C) SEM images of Co<sub>3</sub>Al, CoMn<sub>2</sub>Al and Mn<sub>3</sub>Al LDHs and (D–F) SEM images of the CoMn<sub>2</sub>AlO samples calcined at different temperatures (350, 450 and 550 °C).

Table 1 Physical characterization, catalytic activities,  $E_a$  values and surface elemental compositions of the samples

Sample	BET surface area (m <sup>2</sup> g <sup>-1</sup> )	Pore diameter (nm)	Total pore volume (cm <sup>3</sup> g <sup>-1</sup> )	$D$ (nm)	$T_{10}$ (°C)	$T_{50}$ (°C)	$T_{90}$ (°C)	$E_a$ (kJ mol <sup>-1</sup> )	EDX	XPS Co/Mn
Co <sub>3</sub> AlO	84.63	10.7	0.226	24.9	216	250	285	130.31	Co/Al = 2.86	—
Co <sub>2</sub> MnAlO	121.12	8.1	0.246	21.6	193	232	268	96.03	—	1.87
Co <sub>1.5</sub> Mn <sub>1.5</sub> AlO	127.46	9.0	0.287	18.1	178	220	250	81.91	—	1.02
CoMn <sub>2</sub> AlO	128.04	7.1	0.196	14.6	159	206	238	65.77	Co/Mn = 0.72	0.47
Mn <sub>3</sub> AlO	36.77	24.2	0.222	22.1	184	224	260	93.07	Mn/Al = 2.16	—
CoMn <sub>2</sub> AlO-350	143.81	9.6	0.346	13.8	156	199	227	—	—	0.60
CoMn <sub>2</sub> AlO-550	102.43	12.8	0.328	14.8	142	185	208	—	—	0.43
CoMnAlO film	21.95	6.7	0.037	—	152	205	240	—	—	—

while the structures of the other two samples (at 450 °C and 550 °C) have decomposed to many fine particles.

The microstructures of different oxides are shown in Fig. 4. The TEM images of the catalysts indicate the layered structure of hydrotalcite composed of a number of tiny particles, these catalysts present flattened surfaces and embedded pores in the plate matrix. In addition, many plates have been broken into smaller pieces. From the high-resolution TEM image (Fig. 4(D)) of the  $\text{Co}_3\text{AlO}$  catalyst, the surface lattice spacing is measured to be 0.29 nm corresponding to the (220) crystal plane of  $\text{Co}_3\text{O}_4$  spinel phase. The HRTEM image of the  $\text{CoMn}_2\text{AlO}$  catalyst exposes two identified fringes with lattice spacings of about 0.29 nm and 0.48 nm, rather close to the (220) crystal phase of the  $\text{Co}_3\text{O}_4$  spinel phase with good crystallization and the (101) plane of the  $\text{Mn}_3\text{O}_4$  phase with slightly poor crystallization. The microstructures demonstrate that the  $\text{CoMnAl}$  composite oxide is formed simultaneously during the calcination, which is in agreement with XRD results. It can therefore be stated that the calcination has a great impact on the as-prepared samples and is advantageous for the formation of a solid solution.

To obtain information about the element dispersions, the samples ( $\text{Co}_3\text{AlO}$ ,  $\text{CoMn}_2\text{AlO}$  and  $\text{Mn}_3\text{AlO}$ ) were tested by SEM-EDX analysis (Fig. S1–S3†). The EDX mapping of samples demonstrates uniform distributions of various elements (O, Al, Mn or Co) in the particle region; the related peaks can be seen clearly in the spectra and the proportions of the various elements are listed. The dispersion of Co and Mn further confirms that the results are in agreement with the XRD and TEM analysis.

### 3.3 Temperature-programmed reduction

The reduction behavior and the interaction of various catalysts were examined by using the temperature programmed reduction (TPR) technique in the temperature range from 100 to 800 °C (Fig. 5). Some researchers suggested that the low temperature peak is ascribed to the two-step reduction of relatively large crystalline  $\text{Co}_3\text{O}_4$  particles.<sup>29</sup> The reduction of  $\text{Co}_3\text{O}_4$  usually proceeds *via* the sequence  $\text{Co}_3\text{O}_4 \rightarrow \text{CoO} \rightarrow \text{Co}^0$ .<sup>30</sup> The reduction temperature of  $\text{Co}_3\text{O}_4$  supported on  $\gamma\text{-Al}_2\text{O}_3$  is higher than

that of bulk  $\text{Co}_3\text{O}_4$ , and  $\text{CoAl}_2\text{O}_4$  spinel gives the reduction peak at temperatures as high as  $>800$  °C.<sup>31</sup> For the  $\text{Co}_3\text{AlO}$  catalyst, it is observed that there are three separate reduction peaks with the maximum rates of  $\text{H}_2$  consumption occurring at 255, 360 and 712 °C, respectively. Obviously, the low-temperature peak (150–400 °C) consists of two peaks representing the reduction of  $\text{Co(III)}$  to  $\text{Co(II)}$  and  $\text{Co(II)}$  to  $\text{Co}^0$ .<sup>29</sup> The third separate reduction peak is ascribed to the reduction of the  $\text{CoO}$  or cobalt aluminates at high temperature (500–800 °C),<sup>32</sup> caused by the diffusion of  $\text{Co}^{2+}$  ions into the  $\text{Al}_2\text{O}_3$  support where they may occupy tetrahedral or octahedral lattice sites.<sup>33</sup> The  $\text{Mn}_3\text{AlO}$  sample is reduced in two main temperature regions and the reduction of manganese oxides can be described by the successive reduction processes:  $\text{MnO}_2 \rightarrow \text{Mn}_2\text{O}_3 \rightarrow \text{Mn}_3\text{O}_4 \rightarrow \text{MnO}$ .<sup>26,34</sup> The maximum of the first one (200–350 °C) is around 314 °C, which can be attributed to the reduction of  $\text{MnO}_2$  to  $\text{Mn}_3\text{O}_4$ . The second reduction peak (350–500 °C) is ascribed to the reduction of  $\text{Mn}_3\text{O}_4$  to  $\text{MnO}$ . Except for the  $\text{Mn}_3\text{AlO}$  catalyst, the reduction peaks of the other catalysts are rather similar to the reduction peak of the  $\text{Co}_3\text{AlO}$  catalyst. It is obvious that the peaks in the range 150–500 °C move to lower temperatures, but the third peak shifts to higher temperature with increasing the content of cobalt species (Fig. 5(A)). The reduction of catalyst is becoming easier and the strong interaction of Co and Mn species improves the low temperature reducibility of the  $\text{Co}_{3-x}\text{Mn}_x\text{AlO}$  catalysts. From the reduction peaks (150–500 °C), the  $\text{Co}_{1.5}\text{Mn}_{1.5}\text{AlO}$  and  $\text{CoMn}_2\text{AlO}$  catalysts exhibit lower reduction temperature and higher peak intensity, indicating the improved higher catalytic activity towards VOC oxidation.

Fig. 5(B) presents the  $\text{H}_2$ -TPR profiles of the  $\text{CoMn}_2\text{AlO}$  samples calcined at different temperatures (350, 450 and 550 °C). The  $\text{CoMn}_2\text{AlO}$ -350 catalyst exhibited clear peaks in the lower temperature zone, which can be attributed to the reduction of higher metal ions. However, the reduction temperatures of the  $\text{CoMn}_2\text{AlO}$ -550 sample slightly shift to higher values, which means an increase of oxygen mobility on the catalyst. The oxygen mobility of the catalyst will be an important factor for the catalytic oxidation of benzene.

### 3.4 X-ray photoelectron spectra (XPS)

The surface elemental compositions and the oxidation state of surface species were investigated by X-ray photoelectron

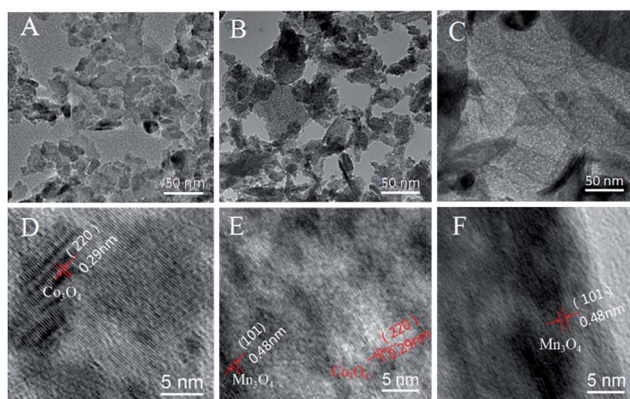


Fig. 4 (A–C) TEM images of the  $\text{Co}_3\text{AlO}$ ,  $\text{CoMn}_2\text{AlO}$  (450 °C) and  $\text{Mn}_3\text{AlO}$  samples; (D–F) the HRTEM images corresponding to A–C, respectively.

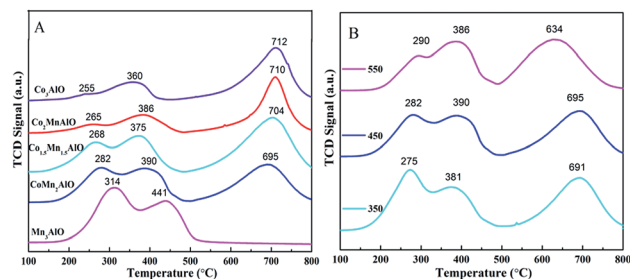


Fig. 5 (A)  $\text{H}_2$ -TPR profiles of  $\text{Co}_{3-x}\text{Mn}_x\text{AlO}$  catalysts and (B)  $\text{H}_2$ -TPR profiles of  $\text{CoMn}_2\text{AlO}$  calcined at different temperature (350, 450 and 550 °C).

spectroscopy (XPS). The Mn 2p, Co 2p and O 1s XPS spectra of the  $\text{Co}_{3-x}\text{Mn}_x\text{AlO}$  catalysts are shown in Fig. 6. As shown in Fig. 6(A), it can be seen that the peaks corresponding to Mn 2p XPS of all samples are asymmetric toward the high binding energy side, and can be broken down into three components. According to the literature,<sup>35</sup> the absence of a satellite peak at +5 eV from the Mn 2p<sub>3/2</sub> peak suggests that no Mn<sup>2+</sup> is present. Hence these three components corresponding to binding energies of 641.2, 642.5 and 644.1 eV can be assigned to the surface Mn<sup>3+</sup> and Mn<sup>4+</sup> species and to the satellite of Mn<sup>3+</sup> species, respectively.<sup>36,37</sup> Moreover, the presence of the two Mn species (Mn<sup>4+</sup> and Mn<sup>3+</sup>) is in agreement with the H<sub>2</sub> consumption peaks in the TPR results. As summarized in Table 2, one can obtain the surface Mn<sup>4+</sup>/Mn<sup>3+</sup> atomic ratios by quantitatively analyzing the XPS spectra of the samples. The appropriate doping cobalt method has a remarkable influence on the surface Mn<sup>4+</sup>/Mn<sup>3+</sup> atomic ratio which increased in the following order:  $\text{CoMn}_2\text{AlO} > \text{Co}_{1.5}\text{Mn}_{1.5}\text{AlO} > \text{Mn}_3\text{AlO} = \text{Co}_2\text{MnAlO}$ . Apparently, the calcination temperature of catalysts has a great impact on the distribution of surface higher Mn<sup>4+</sup> species, increased apparently with increasing the calcination temperature (Fig. 6(B)).

As shown in Fig. 6(C and D), Co 2p XPS spectra are fitted assuming a theoretical value of 2 for the ratio of Co 2p<sub>3/2</sub> and 2p<sub>1/2</sub> and a spin-orbit splitting of 15.2 eV. Generally, the spectra can be broken down into two main components together with four shake-up satellites.<sup>38</sup> The binding energy at 780.2 eV is

ascribed to Co<sup>3+</sup> in octahedral sites, and the binding energy at 781.8 eV and the satellite structure are ascribed to Co<sup>2+</sup> in tetrahedral sites.<sup>39</sup> As summarized in Table 2, the surface Co<sup>3+</sup>/Co<sup>2+</sup> ratios are calculated from the areas by quantitatively analyzing the XPS spectra of the samples. From the areas of the different spin-orbit doublets, the surface Co<sup>3+</sup>/Co<sup>2+</sup> ratio tends to increase with decreasing cobalt. The calcination temperature of catalysts increases the distribution of surface Co<sup>3+</sup> species. According to the TPR profiles of the catalysts, the reduction of higher oxidation states is preferred to take place at lower temperature.

The XPS spectra of O 1s are shown in Fig. 6(E and F). The O 1s peak is curve-fitted with two components at binding energy values of 530.1 and 531.7 eV. The former is due to the surface lattice oxygen (O<sub>latt</sub>) species, whereas the latter is due to the surface adsorbed oxygen (O<sub>ads</sub>) species.<sup>40</sup> The surface molar percentages of O<sub>ads</sub>/O<sub>latt</sub> are summarized in Table 2. The surface O<sub>ads</sub>/O<sub>latt</sub> molar ratio (0.554) of the  $\text{CoMn}_2\text{AlO}$ -550 catalyst is much highest than those of the other samples, indicating that the catalyst has a greater amount of electrophilic oxygen species which can be beneficial for the enhancement in catalytic performance for deep oxidation reactions.

### 3.5 Evaluation of the catalytic behavior

The catalytic performances of the  $\text{Co}_{3-x}\text{Mn}_x\text{AlO}$  catalysts shown in Fig. 7(A) were evaluated using the temperatures of 10% ( $T_{10}$ ), 50% ( $T_{50}$ ), and 90% ( $T_{90}$ ) benzene conversion at a space velocity (SV) of 60 000 mL g<sup>-1</sup> h<sup>-1</sup>. As summarized in Table 1, the order of activity is concluded to be  $\text{CoMn}_2\text{AlO} > \text{Co}_{1.5}\text{Mn}_{1.5}\text{AlO} > \text{Mn}_3\text{AlO} > \text{Co}_2\text{MnAlO} > \text{Co}_3\text{AlO}$ . Apparently, the  $\text{CoMn}_2\text{AlO}$  catalyst is the most active among all the catalysts achieving  $T_{90}$  benzene conversion at 238 °C, while the  $\text{Mn}_3\text{AlO}$  and  $\text{Co}_3\text{AlO}$  catalysts exhibit relatively low activity with only 71% and 35% oxidation of benzene. The reaction rate at  $T_{90} = 238$  °C on  $\text{CoMn}_2\text{AlO}$  is about 0.24 mmol g<sub>cat</sub><sup>-1</sup> h<sup>-1</sup> which is clearly greater than that of  $\text{Mn}_3\text{AlO}$  with 0.19 mmol g<sub>cat</sub><sup>-1</sup> h<sup>-1</sup>, and  $\text{Co}_3\text{AlO}$  with 0.09 mmol g<sub>cat</sub><sup>-1</sup> h<sup>-1</sup>. The CO<sub>2</sub> selectivity was more than 99.0% (Fig. S4<sup>†</sup>). The off-gas was collected using the organic solvent methanol (GC) at different reaction temperatures, and characterized by mass spectrometry (Shimadzu GCMS-QP2010) (Fig. S5<sup>†</sup>). There was no detection of products of incomplete oxidation, indicating that benzene can be completely oxidized over these catalysts. These results indicate the strong interaction of Co and Mn species obviously promotes the catalytic activities of the catalysts compared with  $\text{Mn}_3\text{AlO}$  and  $\text{Co}_3\text{AlO}$  catalysts after the formation of Co, Mn and Al mixed oxides.

The catalytic activities of the  $\text{CoMn}_2\text{AlO}$  catalysts with different calcination temperature (350, 450 and 550 °C) were also characterized, as shown in Fig. 7(B). It is obvious that the  $\text{CoMn}_2\text{AlO}$ -550 catalyst exhibits the highest catalytic activity among all catalysts, achieving complete benzene conversion, and the  $T_{50}$  and  $T_{90}$  values were 185 and 208 °C which were 21 and 30 °C lower than those achieved over the  $\text{CoMn}_2\text{AlO}$ -450 catalyst. It is worth pointing out that the catalytic performance over the  $\text{CoMn}_2\text{AlO}$ -350 catalyst is also higher than that over the  $\text{CoMn}_2\text{AlO}$ -450 catalyst. Meanwhile, the catalytic performance

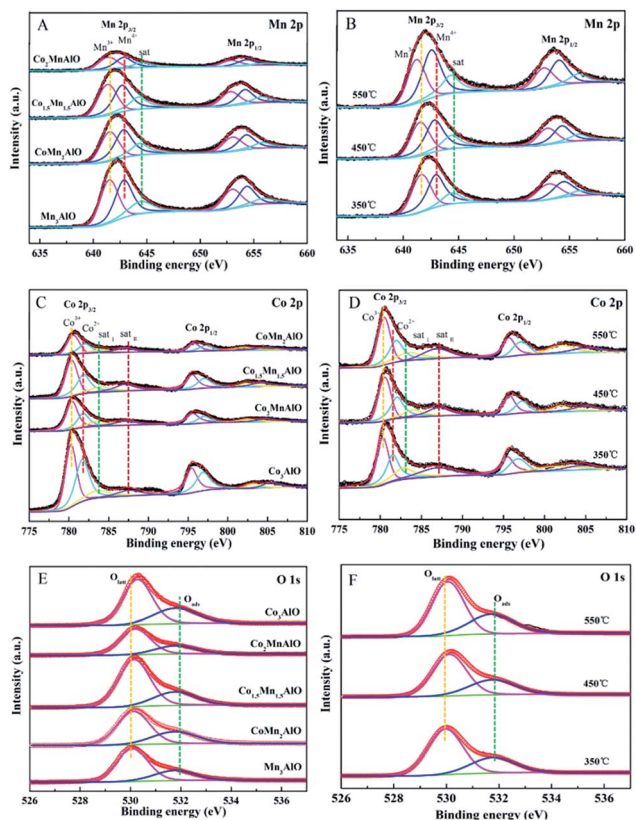


Fig. 6 The Mn 2p, Co 2p and O 1s XPS spectra of the  $\text{Co}_{3-x}\text{Mn}_x\text{AlO}$  catalysts.

Table 2 Surface compositions and oxidation states

Catalysts	Mn 2p			Co 2p			O 1s		
	Mn <sup>3+</sup>	Mn <sup>4+</sup>	Mn <sup>4+</sup> /Mn <sup>3+</sup>	Co <sup>3+</sup>	Co <sup>2+</sup>	Co <sup>3+</sup> /Co <sup>2+</sup>	O <sub>latt</sub>	O <sub>ads</sub>	O <sub>ads</sub> /O <sub>latt</sub>
Co <sub>3</sub> AlO	—	—	—	0.514	0.486	1.06	0.728	0.272	0.41
Co <sub>2</sub> MnAlO	0.492	0.508	1.03	0.526	0.474	1.11	0.732	0.268	0.37
Co <sub>1.5</sub> Mn <sub>1.5</sub> AlO	0.485	0.515	1.06	0.556	0.443	1.25	0.725	0.275	0.38
CoMn <sub>2</sub> AlO	0.452	0.548	1.21	0.568	0.432	1.31	0.703	0.297	0.42
Mn <sub>3</sub> AlO	0.492	0.508	1.03	—	—	—	0.709	0.291	0.37
CoMn <sub>2</sub> AlO-350	0.431	0.569	1.31	0.558	0.442	1.26	0.671	0.329	0.49
CoMn <sub>2</sub> AlO-550	0.471	0.530	1.12	0.579	0.421	1.37	0.708	0.179	0.55

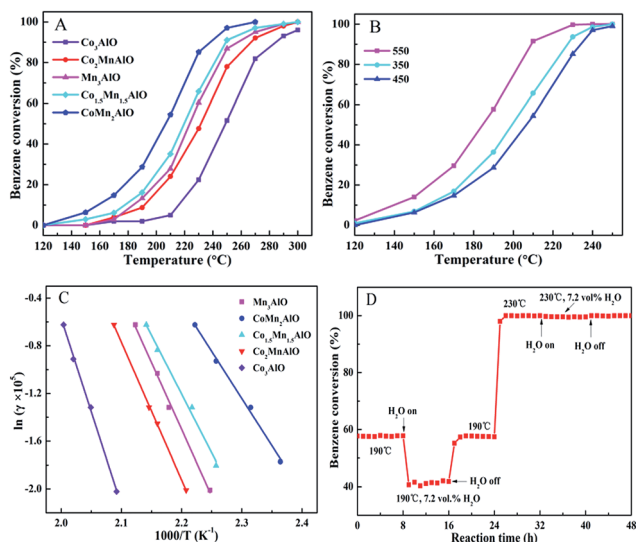


Fig. 7 (A) Benzene conversion as a function of reaction temperature over Co<sub>3-x</sub>Mn<sub>x</sub>AlO catalysts; (B) benzene conversion over CoMn<sub>2</sub>AlO catalysts calcined at different temperatures (350, 450 and 550 °C); (C) Arrhenius plots for the oxidation of benzene over the Co<sub>3-x</sub>Mn<sub>x</sub>AlO catalysts; (D) effect of water vapor on the activities of CoMn<sub>2</sub>AlO-550 catalysts at 190 °C and 230 °C. Benzene concentration = 100 ppm, water concentration = 7.2 vol% and SV = 60 000 mL g<sup>-1</sup> h<sup>-1</sup>.

of the CoMn<sub>2</sub>AlO-550 catalyst is similar to the three-dimensional manganese oxides prepared by the oxalate route with  $T_{90}$  around 209 °C, probably due to 2D mesoporous metal oxides being convenient for rapid and homogeneous oxygen diffusion throughout the whole surface of the catalysts, which can provide many active sites for catalytic reactions.<sup>27,41</sup> Obviously, the catalytic activity over the CoMn<sub>2</sub>AlO-550 catalyst is much better than other reported literature,<sup>9,42-45</sup> such as MnCe(18 : 1)/Al-PILC ( $T_{90}$  = 290 °C), Mn/Al-PILC ( $T_{90}$  = 340 °C), Co<sub>3</sub>AlO ( $T_{90}$  = 300 °C) Co/CeO<sub>2</sub>/SBA-15 ( $T_{90}$  = 265 °C), CeO<sub>2</sub>-MnO<sub>x</sub> ( $T_{90}$  = 375 °C) and 0.5% Pt/Al<sub>2</sub>O<sub>3</sub> ( $T_{90}$  = 260 °C). Obviously, the relatively lower reaction temperature among the reported catalysts makes CoMnAlO a promising catalyst for benzene combustion.

The catalytic performance can also be evaluated by comparing the  $E_a$  values of different catalysts, and the sample with lower  $E_a$  value will exhibit superior catalytic activity. The catalytic oxidation of benzene in the presence of excess oxygen

follows first-order and zero-order kinetics with respect to the benzene concentration and oxygen concentration, respectively.<sup>46</sup> It is reasonable to assume that in the case of excess oxygen the reaction should obey first-order kinetics, and the equations are as follows:

$$\gamma_{C_6H_6} = \frac{N_{C_6H_6} \times \eta_{C_6H_6}}{W_{cat}}$$

$$\gamma_{C_6H_6} = -\kappa c = \left[ -A \exp\left(-\frac{E_a}{RT}\right) \right] c$$

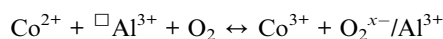
where  $N_{C_6H_6}$  is the C<sub>6</sub>H<sub>6</sub> gas flow rate (mol s<sup>-1</sup>),  $W_{cat}$  is the catalyst weight (g), and  $\gamma$ ,  $\kappa$ ,  $A$ , and  $E_a$  are the reaction rate ( $\mu\text{mol g}^{-1} \text{s}^{-1}$ ), rate constant (s<sup>-1</sup>), pre-exponential factor, and apparent activation energy (kJ mol<sup>-1</sup>), respectively. The  $\kappa$  values can be calculated from the reaction rates and reactant conversions.

The Arrhenius plots for the oxidation of benzene at a benzene conversion <20% are displayed in Fig. 7(C). The plots of  $\ln(\gamma \times 10^5)$  versus  $1000/T$  perform excellent linear relationships with the correlation coefficients ( $R^2$ ) were rather close to 1 and the activation energies ( $E_a$ ) based on the slopes of the Arrhenius plots are listed in Table 1. The results indicate that the  $E_a$  values decreased in the following order: Co<sub>3</sub>AlO > Co<sub>2</sub>-MnAlO > Mn<sub>3</sub>AlO > Co<sub>1.5</sub>Mn<sub>1.5</sub>AlO > CoMn<sub>2</sub>AlO, which confirms the promoting effect of Co species.

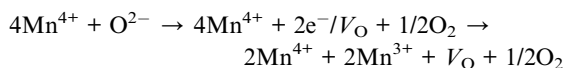
To examine the stability and effect of water vapor on the catalytic performances of the CoMn<sub>2</sub>AlO-550 catalyst, the on-stream reactions at different temperatures (190 and 230 °C) were carried out in the absence and presence of 7.2 vol% water vapor as shown in Fig. 7(D). When 7.2 vol% H<sub>2</sub>O was introduced into the stream at 190 °C, the benzene conversion decreased sharply from 57.8 to 41.5% within 8 h. When the water vapor was cut off, the benzene conversion at 190 °C nearly recovered. Then the on-stream reaction was continued, adjusting the temperature from 190 °C to 230 °C. The benzene conversion was unchanged with 99.8% with or without the water vapor. These results suggest that in spite of the competitive adsorption of water and benzene molecules on the active sites, the CoMn<sub>2</sub>AlO-550 catalyst can tolerate the presence of water vapor and maintain excellent catalytic activity at high temperature. The catalyst with stronger oxygen mobility can more easily activate

oxygen molecules at a relatively higher temperature, where the adsorption of oxygen is stronger than that of water.<sup>47</sup>

It is noticeable that the catalytic activity of a transition metal oxide is associated with several factors, such as the distribution of surface species, oxygen vacancies, reducibility, surface area, and morphology. A catalyst with a higher surface area should show better catalytic activity. Thus, the CoMn<sub>2</sub>AlO-350 catalyst exhibited higher activity at lower temperature than the CoMn<sub>2</sub>AlO-450 catalyst due to its higher surface area. However, it seems that the CoMn<sub>2</sub>AlO-550 catalyst with slightly lower surface area exhibits higher specific activity, which is similar to other report.<sup>8</sup> The homogeneous distributions of various elements could greatly improve the dispersion of active species. Amorphous Al<sub>2</sub>O<sub>3</sub> dispersed in the particle region makes the structure difficult to damage at high temperature, making the active elements remain very well dispersed. It is well known that an increased amount of structural defects, which is beneficial for the activation of oxygen molecules to active oxygen adspecies, and low temperature reducibility result in better catalytic performance.<sup>48</sup> The structural defects of the spinel Co<sub>3</sub>O<sub>4</sub> lattice could play a key role in creating oxygen vacancies on the surface, which might be favorable for accelerating the adsorption and dissociation of oxygen molecules, hence resulting in the formation of highly active electrophilic oxygen species. Meanwhile, when the content of high valence metal ions increases, the chemical potential and reactivity of oxygen adjacent to the metal ions will be promoted. Gabrovská<sup>49</sup> proposed an active assembly formed by the redox couple Co<sup>3+</sup>/Co<sup>2+</sup> and O<sub>2</sub><sup>x-</sup> radicals stabilized on Al<sup>3+</sup> ion for CO oxidation:



where  $\square\text{Al}^{3+}$  represents an anion vacancy close to an Al<sup>3+</sup> ion. The adsorbed oxygen can be promoted by increasing the content of higher manganese oxidation state (Mn<sup>4+</sup>) based on the principle of electro-neutrality. A lower manganese state (Mn<sup>3+</sup>) existing in the crystal will produce oxygen vacancies (V<sub>O</sub>), which will promote the mobility of lattice oxygen. Surface oxygen vacancies will be generated to maintain electrostatic balance according to the following process:



Based on XPS spectra results, the catalytic activity of benzene oxidation is influenced by various factors (Mn<sup>4+</sup>/Mn<sup>3+</sup>, Co<sup>3+</sup>/Co<sup>2+</sup>, O<sub>ads</sub>/O<sub>latt</sub> and synergetic effect of Co and Mn). The sample with higher Mn<sup>4+</sup>/Mn<sup>3+</sup> molar ratio with the lower thermal treatment temperature will contain more adsorbed oxygen species, and the physically adsorbed oxygen and chemically adsorbed oxygen species are relatively easier to desorb. The adsorbed surface oxygen is responsible for the high catalytic activity of CoMn<sub>2</sub>AlO-550 in the oxidation of benzene due to the high crystallinity of samples with a high content of lattice defects and the good synergistic effect between cobalt and manganese at high temperature. Furthermore, the XPS results

demonstrate the electronic transfer between cobalt and manganese to provide a redox mechanism: Co<sup>3+</sup>-Mn<sup>3+</sup> ↔ Co<sup>2+</sup>-Mn<sup>4+</sup> which is critical to catalytic reaction after the formation of Co and Mn mixed oxides.

### 3.6 The structure and catalytic performance of the monolithic CoMnAlO film catalyst

Taking into account the practical application of catalysts, the monolithic catalyst on the Al substrate was used to replace powder samples with better heat conduction. As we can see, the CoMnAl LDH film crystallized as thin curved and hydroxalate-like platelets with the *ab* plane in a perpendicular orientation to the support (Fig. 8(D)), and two sharp diffraction lines corresponding to aluminum are found in the XRD pattern of the dried sample (Fig. 8(A)). The XRD patterns of the monolithic CoMnAlO film catalyst and its LDH precursor show a series of diffraction peaks, which are similar to those of their powder samples. The photograph of the sample shows that the film is regular and adhesive to the Al substrate (Fig. 8(C)). The amount of CoMnAlO film catalyst grown on the Al substrate (4 × 15 cm) is more than 0.08 g. As shown in Fig. 8(B), the catalytic activity of the CoMnAlO film is a little reduced for benzene conversion with T<sub>90</sub> at 240 °C compared with the corresponding CoMn<sub>2</sub>AlO powder catalyst with T<sub>90</sub> at 208 °C. However, the monolithic catalyst with more active sites exposed exhibits a reaction rate of 1.19 mmol g<sup>-1</sup> h<sup>-1</sup> at T<sub>90</sub>, much higher than that of 0.24 mmol g<sup>-1</sup> h<sup>-1</sup> over the CoMn<sub>2</sub>AlO-550 powder sample. Compared with films prepared by colloidal deposition techniques, thin films growing directly from the Al substrate can have better adhesion and mechanical stability. The mechanism of oxidation supposes adsorption of organic compounds on the catalyst surface, and the activation of adsorbed oxygen

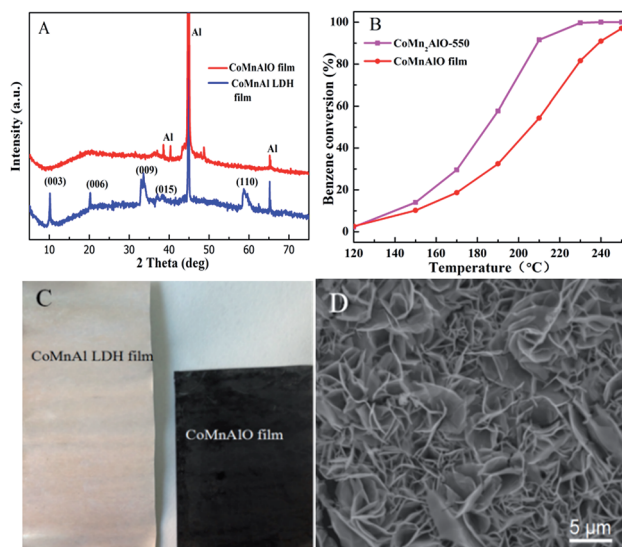
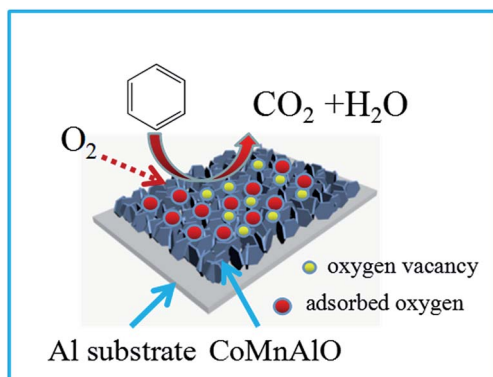


Fig. 8 (A) XRD patterns of the monolithic CoMnAl LDH film and CoMnAlO film catalyst on the Al substrate, (B) the comparison of the benzene conversion over CoMnAlO film and CoMn<sub>2</sub>AlO-550 powder catalyst, (C) photograph and (D) SEM image of the CoMnAl LDH film precursor on the Al substrate.



Scheme 1 The pathway for benzene oxidation and the structure of the CoMnAlO film catalyst.

molecules to active oxygen adspecies. Scheme 1 shows the possible pathway for benzene oxidation on the CoMnAlO film catalyst. It is worth taking into account the practical application of the film catalyst in total oxidation of benzene.

## 4. Conclusions

A series of mesoporous and dispersed  $\text{Co}_{3-x}\text{Mn}_x\text{AlO}$  composited metal oxide catalysts have been successfully fabricated on layered double hydroxide (LDH) precursors. The  $\text{Co}_{3-x}\text{Mn}_x\text{AlO}$  catalyst obviously promotes the catalytic activities towards benzene oxidation, compared with single  $\text{Co}_3\text{AlO}$  and  $\text{Mn}_3\text{AlO}$  catalysts. The catalytic performance was associated with low temperature reducibility, high surface areas and surface  $\text{Mn}^{4+}/\text{Mn}^{3+}$ ,  $\text{Co}^{3+}/\text{Co}^{2+}$  and  $\text{O}_{\text{ads}}/\text{O}_{\text{latt}}$  species. The  $\text{CoMn}_2\text{AlO}$ -550 catalyst exhibited higher catalytic activity because it possesses the highest low temperature reducibility, the most abundant surface  $\text{Co}^{3+}$ ,  $\text{Mn}^{4+}$  and  $\text{O}_{\text{ads}}$  species, and it tolerates the highest concentration of water vapor. Moreover, the monolithic CoMnAlO film catalyst on the Al substrate exhibited high catalytic efficiency, which provides great potential for their practical application.

## Acknowledgements

This research was supported by the National Natural Science Foundation of China (No. 21401200), and the strategic project of science and technology of Chinese Academy of Sciences (No. XDB05050000).

## Notes and references

- R. Atkinson, *Atmos. Environ.*, 2000, **34**, 2063–2101.
- T. Lindgren, *Build. Environ.*, 2010, **45**, 596–600.
- A. Maudhuit, C. Raillard, V. Héquet, L. Le Coq, J. Sablayrolles and L. Molins, *Chem. Eng. J.*, 2011, **170**, 464–470.
- J. E. Cometto-Muñiz, W. S. Cain and M. H. Abraham, *Indoor Air*, 2004, **14**(s8), 108–117.
- K. Everaert and J. Baeyens, *J. Hazard. Mater.*, 2004, **109**, 113–139.
- Z. Zhao, X. Lin, R. Jin, G. Wang and T. Muhammad, *Appl. Catal., B*, 2012, **115–116**, 53–62.
- K. Karásková, L. Obalová, K. Jiráťová and F. Kovanda, *Chem. Eng. J.*, 2010, **160**, 480–487.
- D. Delimaris and T. Ioannides, *Appl. Catal., B*, 2008, **84**, 303–312.
- S. Zuo, Q. Huang, J. Li and R. Zhou, *Appl. Catal., B*, 2009, **91**, 204–209.
- Y. Zhang, Z. Qin, G. Wang, H. Zhu, M. Dong, S. Li, Z. Wu, Z. Li, Z. Wu, J. Zhang, T. Hu, W. Fan and J. Wang, *Appl. Catal., B*, 2013, **129**, 172–181.
- J. Luo, M. Meng, X. Li, X. Li, Y. Zha, T. Hu, Y. Xie and J. Zhang, *J. Catal.*, 2008, **254**, 310–324.
- C. Ma, D. Wang, W. Xue, B. Dou, H. Wang and Z. Hao, *Environ. Sci. Technol.*, 2011, **45**, 3628–3634.
- E. Genty, R. Cousin, S. Capelle, C. Gennequin and S. Siffert, *Eur. J. Inorg. Chem.*, 2012, **2012**, 2802–2811.
- S. Li, H. Wang, W. Li, X. Wu, W. Tang and Y. Chen, *Appl. Catal., B*, 2015, **166–167**, 260–269.
- (a) C. Gennequin, S. Siffert, R. Cousin and A. Aboukaïs, *Top. Catal.*, 2009, **52**, 482–491; (b) C. Gennequin, R. Cousin, J. F. Lamonier, S. Siffert and A. Aboukaïs, *Catal. Commun.*, 2008, **9**, 1639–1643.
- S. He, Z. An, M. Wei, D. G. Evans and X. Duan, *Chem. Commun.*, 2013, **49**, 5912–5920.
- J. Feng, Y. He, Y. Liu, Y. Du and D. Li, *Chem. Soc. Rev.*, 2015, **44**, 5291–5319.
- J.-F. Lamonier, A.-B. Boutoundou, C. Gennequin, M. J. Pérez-Zurita, S. Siffert and A. Aboukaïs, *Catal. Lett.*, 2007, **118**, 165–172.
- H. Chen, F. Zhang, S. Fu and X. Duan, *Adv. Mater.*, 2006, **18**, 3089–3093.
- F. Kovanda, K. Jiráťová, J. Ludvíková and H. Raabová, *Appl. Catal., A*, 2013, **464–465**, 181–190.
- S. Aisawa, H. Hirahara, H. Uchiyama, S. Takahashi and E. Narita, *J. Solid State Chem.*, 2002, **167**, 152–159.
- Z. Liu, R. Ma, M. Osada, N. Iyi, Y. Ebina, K. Takada and T. Sasaki, *J. Am. Chem. Soc.*, 2006, **128**, 4782–4880.
- Y. Shao, J. Li, H. Chang, Y. Peng and Y. Deng, *Catal. Sci. Technol.*, 2015, **5**, 3536–3544.
- J. Cheng, J. Yu, X. Wang, L. Li, J. Li and Z. Hao, *Energy Fuels*, 2008, **22**, 2131–2137.
- S. Zhao, K. Li, S. Jiang and J. Li, *Appl. Catal., B*, 2016, **181**, 236–248.
- W. Tang, X. Wu, D. Li, Z. Wang, G. Liu, H. Liu and Y. Chen, *J. Mater. Chem. A*, 2014, **2**, 2544.
- M. B. Zakaria, M. Hu, R. R. Salunkhe, M. Pramanik, K. Takai, V. Malgras, S. Choi, S. X. Dou, J. H. Kim, M. Imura, S. Ishihara and Y. Yamauchi, *Chem.–Eur. J.*, 2015, **21**, 3605–3612.
- M. B. Zakaria, M. Hu, N. Hayashi, Y. Tsujimoto, S. Ishihara, M. Imura, N. Suzuki, Y.-Y. Huang, Y. Sakka, K. Ariga, K. C. W. Wu and Y. Yamauchi, *Eur. J. Inorg. Chem.*, 2014, **2014**, 1137–1141.
- B. de Rivas, R. López-Fonseca, C. Jiménez-González and J. I. Gutiérrez-Ortiz, *J. Catal.*, 2011, **281**, 88–97.
- H. Lin and Y. Chen, *Mater. Chem. Phys.*, 2004, **85**, 171–175.

- 31 Y. Ji, Z. Zhao, A. Duan, G. Jiang and J. Liu, *J. Phys. Chem. C*, 2009, **113**, 7186–7199.
- 32 P. Li, C. He, J. Cheng, C. Y. Ma, B. J. Dou and Z. P. Hao, *Appl. Catal., B*, 2011, **101**, 570–579.
- 33 R. L. Chln and D. M. Hercules, *J. Chem. Phys.*, 1982, **86**, 360–367.
- 34 V. P. Santos, M. F. R. Pereira, J. J. M. Órfão and J. L. Figueiredo, *Appl. Catal., B*, 2010, **99**, 353–363.
- 35 B. Kucharczyk and W. Tylus, *Appl. Catal., A*, 2008, **335**, 28–36.
- 36 Q. Ye, J. Zhao, F. Huo, D. Wang, S. Cheng, T. Kang and H. Dai, *Microporous Mesoporous Mater.*, 2013, **172**, 20–29.
- 37 G. Liu, J. Li, K. Yang, W. Tang, H. Liu, J. Yang, R. Yue and Y. Chen, *Particuology*, 2015, **19**, 60–68.
- 38 B. Puértolas, A. Smith, I. Vázquez, A. Dejoz, A. Moragues, T. Garcia and B. Solsona, *Chem. Eng. J.*, 2013, **229**, 547–558.
- 39 J. Zhong, A. Wang, G. Li, J. Wang, Y. Ou and Y. Tong, *J. Mater. Chem.*, 2012, **22**, 5656.
- 40 Y. Jiang, Y. Li, M. Yan and N. Bahlawane, *J. Mater. Chem.*, 2012, **22**, 16060.
- 41 M. B. Zakaria, M. Hu, M. Pramanik, C. L. Li, J. Tang, A. Aldalbahi, S. M. Alshehri, V. Malgras and Y. Yamauchi, *Chem.–Asian J.*, 2015, **10**, 1541–1545.
- 42 D. Li, Y. Ding, X. Wei, Y. Xiao and L. Jiang, *Appl. Catal., A*, 2015, **507**, 130–138.
- 43 Z. Mu, J. J. Li, M. H. Duan, Z. P. Hao and S. Z. Qiao, *Catal. Commun.*, 2008, **9**, 1874–1877.
- 44 Z. Wang, G. Shen, J. Li, H. Liu, Q. Wang and Y. Chen, *Appl. Catal., B*, 2013, **138–139**, 253–259.
- 45 J. Hou, Y. Li, L. Liu, L. Ren and X. Zhao, *J. Mater. Chem. A*, 2013, **1**, 6736.
- 46 M. Alifanti, M. Florea, S. Somacescu and V. I. Parvulescu, *Appl. Catal., B*, 2005, **60**, 33–39.
- 47 Y. Liu, H. Dai, J. Deng, S. Xie, H. Yang, W. Tan, W. Han, Y. Jiang and G. Guo, *J. Catal.*, 2014, **309**, 408–418.
- 48 F. Wang, H. Dai, J. Deng, G. Bai, K. Ji and Y. Liu, *Environ. Sci. Technol.*, 2012, **46**, 4034–4041.
- 49 M. Gabrovska, R. Edreva-Kardjieva, K. Tenchev, P. Tzvetkov, A. Spojakina and L. Petrov, *Appl. Catal., A*, 2011, **399**, 242–251.